Supporting Information

N-doped microporous carbons derived from direct carbonization of K⁺ exchanged meta-aminophenol-formaldehyde resin for superior CO₂ sorption

Jin Zhou,[a] Zhaohui Li,[a] Wei Xing,[b] Tingting Zhu,[a] Honglong Shen,[a] and Shuping Zhuo[a*]*

[a] School of Chemical Engineering, Shandong University of Technology, Zibo 255049, P. R. China. Tel. /fax: +86 533 2781664

[b] School of Science, State Key Laboratory of Heavy Oil Processing, China University of Petroleum Qingdao 266580 (P. R. China). Fax: (+) +86-533-86983579

Corresponding author: S. Zhuo, E-mails: zhuosp_academic@yahoo.com

W. Xing, E-mails: xingwei@upc.edu.cn

Contents:

1. Preparation of NMC-x

In a typical synthesis, 1.10 g meta-aminophenol (10 mmol) and 0.56 g KOH (10 mmol) were dissolved into 5 mL H_2O, and stirred for 1 h to form a pale yellow clear solution. Afterward, 1.60 g formalin (37%, 20 mmol formaldehyde) was added into the above solution and stirred for ca. 30 min at 25 °C. The solution was then sealed and transferred into an oven at 80°C. The solution quickly turned red and solidified within 30 min. After curing for 72 h, the obtained dark red hydrogel was immersed in acetone for three days in which fresh acetone were replaced daily. The washed hydrogels were dried under flow air to give dark red xerogels (Fig. S1). For carbonization, the xerogels were heated under Ar atmosphere to 200 °C with a heating rate of 2 °C min^{-1}, then maintained at 200 °C for 1h, and subsequently heated to a certain temperature with a heating rate of 5 °C min^{-1} and kept at this temperature for 1.5 hours. Finally, the N-doped microporous carbons (NMC-x, where x designates the final heating temperature in °C) were liberated by washing with dilute HCl (10 wt%) and deionized water to neutrality.

2. Characterization of NMC-x

Microscopic morphology of the prepared carbon materials were observed with a scanning electron microscope (SEM, Sirion 200 FEI Netherlands) and a transmission electron microscope (JEM2100, JEOL, Japan). Surface chemical properties were determined by X-ray photoelectron spectroscopy (XPS, Escalab 250, USA). X-ray diffraction (XRD) patterns were conducted by using a Brucker D8 Advance diffractometer with Cu Kα radiation. Raman spectra were collected by a LabRAM HR800 from JY Horiba. The element contents and C/H/N ratios of NMC-x were determined by a Vario ELcube elemental analysis system.

3. Sorption measurement:

All the gas sorption measurements were conducted on a Micromeritics ASAP 2020 static volumetric analyzer. The samples were degassed at 150 °C overnight before sorption measurements. The surface area and pore size distribution (PSD) of the NMC-x were analysed by means of N_2 sorption at -196 °C and CO_2 adsorption at 0 °C. The BET (Brunauer-Emmett-Teller) surface area (S_{BET}) and Langmuir surface area (S_L) were calculated using the N_2 adsorption isotherm data within the relative pressure ranging from 0.05 to 0.25. Total pore volume (V_T) was obtained at a relative pressure of 0.995. For the calculation of PSD, nonlocal density functional theory (NLDFT) models are widely applied, and featured in a standard by ISO (*ISO-15901-3: Pore size distribution and porosity of solid materials by mercury porosimetry and gas adsorption– Part3: Analysis of micropores by gas adsorption.*). Standard NLDFT models assume an idealized flat-graphitic-like surface. In contrast to NLDFT models, quenched solid density functional theory (QSDFT) models take into account carbon surface roughness features. According to several previous reports[1-3], the chosen NLDFT models may not describe all the subtleties of a real carbon surface. QSDFT models provide a better representation of the surface properties, including surface roughness features. However, QSDFT models are not yet available for all of the different measurement conditions (e.g., CO_2, 0 °C). Thus, in this work, the pore size distributions of NMC-x were determined by using QSDFT methods considering sorption of nitrogen at -196 °C in carbon as a model adsorbent and slit-like pores as a pore model, or in the case of CO_2 (0 °C), NLDFT methods for carbon with slit-like pores as a pore model. The implemented QSDFT models were supplied by Quantachrome Autosorb iQ2.02 software. The CO_2 sorption experiments were performed at different temperatures.

4. Analysis of the narrow microporosity by Dubinin−Radushkevich equation:

The CO_2 adsorption data obtained at 0°C were used to analyze the narrow microporosity by means of the Dubinin−Radushkevich (D−R) equation[4, 5]:

$$V = V_0 \exp\{-k(RT/\beta)^2[2.303\lg(P_0/P)]^2\} \qquad (1)$$

where V (cm^3 g^{-1}) is the volume filled at a temperature T and the relative pressure (P/P_0), V_0 (cm^3 g^{-1}) is the micropore volume, and k and β are a constant about the pore structure and the affinity coefficient ($\beta = 0.35$ for CO_2), respectively. The average micropore width, L (nm), was calculated

by means of the empirical correlation proposed by Stoeckli et al. [6]:

$$L = 10.8/(E_0 - 11.4) \qquad (2)$$

where E_0 is the characteristic energy.

5. Calculation of heats of adsorption:

The isosteric heats of adsorption (Q_{st}) were calculated according to Clausius-Clapeyron equation:

$$\ln\left(\frac{p_1}{p_2}\right) = Q_{st} \times \frac{T_2 - T_1}{R \times T_1 \times T_2} \qquad (3)$$

where Q_{st} is the isosteric heats of adsorption, T_i represents a temperature at which an isotherm i is measured, p_i represents a pressure at which a specific equilibrium adsorption amount is reached at T_i, R is gas constant (8.314 J K^{-1} mol^{-1}).

Table S1 Texture properties and element compositions of NMC-*x* samples

Sample	N$_2$ adsorption at -196 °C					CO$_2$ adsorption at 0 °C		
	S_{BET}	S_{micro}	V_{total}	V_{micro}	S_L	V_0	E_0	L
	(m^2 g^{-1})	(m^2 g^{-1})	(cm^3 g^{-1})	(cm^3 g^{-1})	(m^2 g^{-1})	(cm^3 g^{-1})	(kJ mol^{-1})	(nm)
NMC-600	272	270	0.15	0.14	397	0.26	32.85	0.50
NMC-700	518	498	0.27	0.26	746	0.29	32.54	0.51
NMC-800	603	589	0.31	0.30	877	0.35	31.31	0.54
NMC-900	664	641	0.34	0.33	934	0.36	29.88	0.58

*Brunauer–Emmett–Teller (BET) surface area (S_{BET}) and Langmuir surface area (S_L) were calculated using the N$_2$ adsorption isotherm data within the relative pressure range of 0.05–0.25. Total pore volume (V_T) was obtained at $P/P_0 = 0.995$. Micropore volume (V_{micro}) was calculated by *t*-plot method. Mesopore volume (V_{meso}) was determined by subtracting the micropore volume from the total pore volume. E_0 is the characteristic energy, V_0 (cm^3 g^{-1}) is the micropore volume, L is the average micropore width calculated by means of the empirical correlation proposed by Stoeckli et al (vide infra).

Table S2 N-containing groups on the surface of NMC-*x* samples

Sample	C (at%)	O (at%)	Nitrogen species (at%)				
			total	pyridinic-N	-C=NH	pyrrolic N	quaternary N
NMC-600	84.0	12.2	3.8	0.6	0.2	1.5	1.5
NMC-700	84.2	12.3	3.5	0.8	0.2	1.6	0.7
NMC-800	87.5	9.3	3.2	1.0	0.4	0.7	1.4
NMC-900	88.1	10.6	1.3	0.3	0.3	0.2	0.5

Table S3 Element analysis of NMC-*x* samples

Sample	Element content (wt%)			C/ H	C/ N
	C	H	N		
NMC-600	74.32	2.05	6.33	36.2	11.7
NMC-700	78.26	1.95	6.06	40.1	12.9
NMC-800	79.14	1.56	4.24	50.7	18.7
NMC-900	83.76	0.93	2.34	90.1	35.8

The results of element analysis indicate that the elements of H and N are eliminated during the high temperature carbonization procedure. The ratios of C/H and C/N of NMCs increase with the rise of carbonization temperature, which clearly shows that the carbonization degree increases with the rise of carbonization temperature. Note that the N contents determined by element analysis are higher than those determined by XPS, which may be due to the different working mechanism between elemental analysis and XPS. In detail, element analysis gives a quantitative determination of element content in the whole body of materials or compounds, while XPS only gives an elemental composition of the surface (top 0–10 nm usually).

Table S4 CO_2 sorption capacities of NMC-*x* at different temperatures and pressures

Sample	CO_2 sorption capacity (mmol g^{-1})		
	0 °C P =1 bar	25 °C P =1 bar	25 °C P =0.15 bar
NMC-600	4.5	3.9	1.67
NMC-700	4.4	3.6	1.4
NMC-800	5.1	4.0	1.6
NMC-900	5.1	3.9	1.4

Table S5 CO_2 uptake values of various porous carbon materials at 25 °C

| Materials	Porosity		CO_2 uptake (mmol g^{-1})		Reference
	S_{BET} (m^2 g^{-1})	V_{total} (cm^3 g^{-1})	1 bar	0.15 bar	
NMC-600	**272**	**0.15**	**3.9**	**1.67 (1.95, 0.20 bar)**	**This study**
NMC-800	**603**	**0.31**	**4.0**	**1.6**	**This study**
activated carbon	2829	1.55	2.92	N.A.	[7]
HCM-DCH-1	670	0.46	2.6	~1.0	[8]
PCN-71	610	0.31	2.88	~1.0	[9]
CS-6	530	0.23	3.8	<1.5	[10]
CS3-6A	1184	0.37 (<1.0 nm)	4.1	<1.5	[11]
N-doped ZTCs	3360	1.71	4.38	<1.0	[12]
PAF-1/C-900	1174	N.A.	4.1	~1.3	[13]
ACFK-3	2180	1.00	5.7	1.6	[14]
CS-8	669	0.29	3.0	1.42	[15]
KOH-activated OMC	1820	0.95	3.4	<1.0	[16]
KOH-activated graphite nanofibers	567	0.71	1.35	<0.5	[17]
CP-2-600	1700	0.88	3.9	~1.0	[18]
N-doped porous carbon monoliths	464	0.23	3.13	N.A.	[19]
NAC	2546	1.47	3.75	N.A.	[7]
porous carbon nitride spheres	550	0.90	2.90	N.A.	[20]
IBN9-NC1-A	1181	0.73	4.50	1.75(0.2bar)	[21]
PC-1	1600	0.72	3.5	~1.0	[22]
MFB-600	490	0.91	2.25	N.A.	[23]
AS-2-600	1260	0.62	4.8	~1.2	[24]
ZIF-81 ZIF-82 ZIF-95			2.2		[25, 26]
CPF-6 (with 67% of N-donor sites)			4.5 (0 °C)		[27]
bio-MOF-11			4.1		[28]
SK-0.3-700	1060	0.52	4.24	1.2	[29]
SK-0.5-600	710	0.44	3.60	1.3	[29]
AC-750-0.5	1060	0.52	4.30	1.38	[30]
AC-700-1	1685	0.94	4.10	0.93	[30]

N.A means not available.
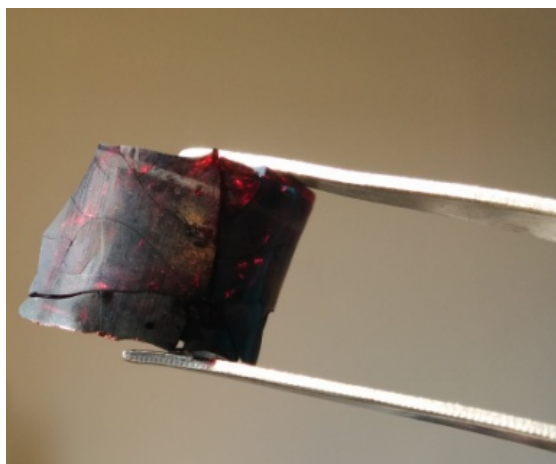
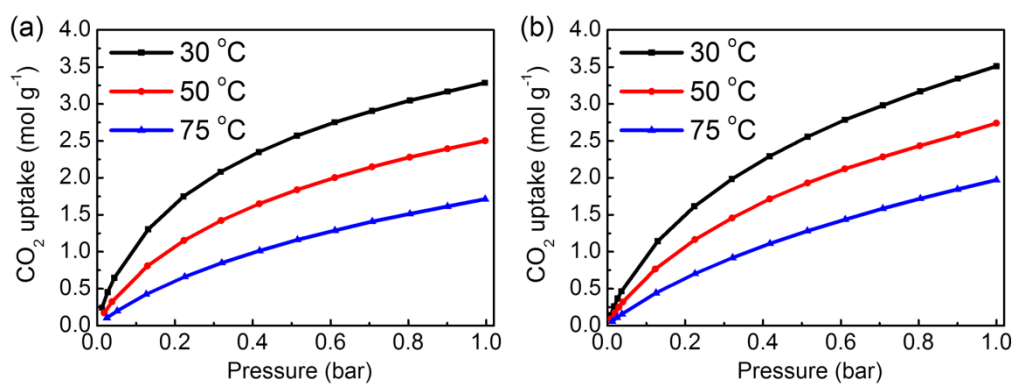**Fig. S1 Digital camera** image of xerogels
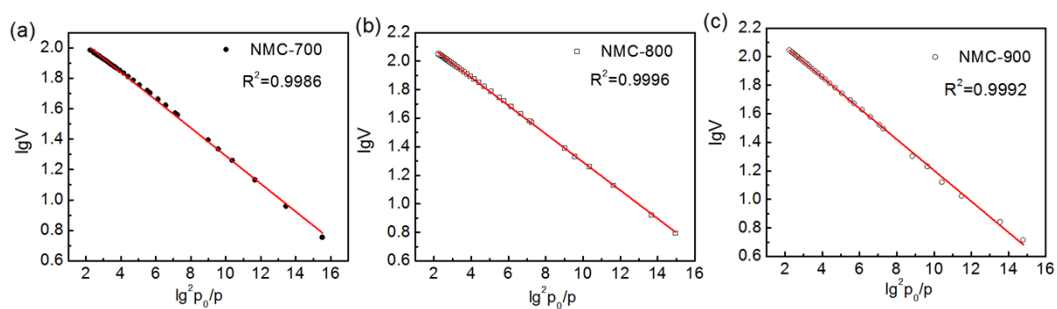
Fig. S2 D-R plots for CO_2 sorption by (a) NMC-700, (b) NMC-800 and (c) NMC-900
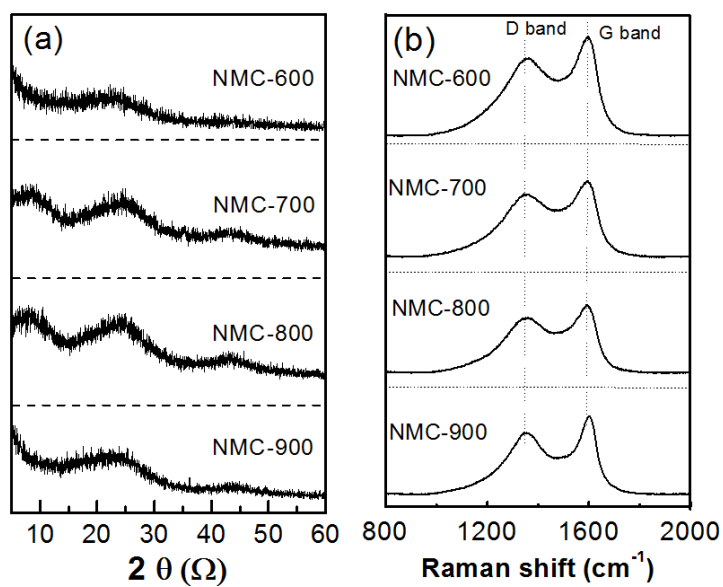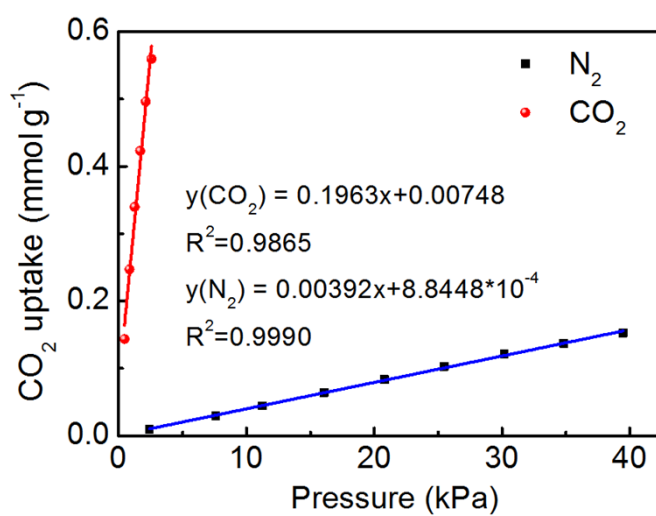

Fig. S3 (a) Raman spectra and (b) XRD patterns of NMC-x
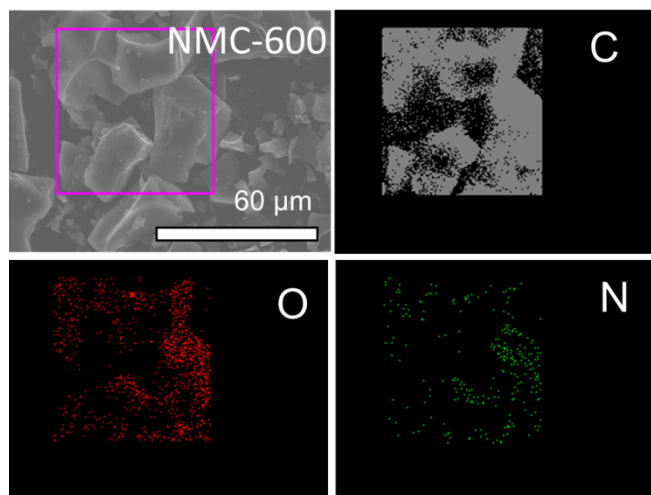
Fig. S4 EDS mapping of NMC-600

Fig. S5 CO_2 sorption isotherms at elevated temperature (a) NMC-600, (b) NMC-800

$y(CO_2) = 0.1963x+0.00748$

$R^2=0.9865$

$y(N_2) = 0.00392x+8.8448*10^{-4}$

$R^2=0.9990$

Fig. S6 Initial slope calculation for CO_2 and N_2 isotherms collected at 25°C
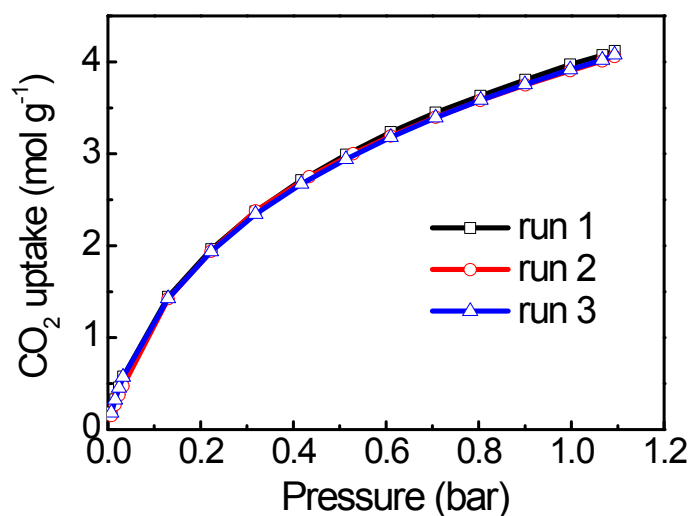
Fig. S7 Regeneration of NMC-800 for CO_2 uptake at 25 °C

References:

1. G. Y. Gor, M. Thommes, K. A. Cychosz and A. V. Neimark, *Carbon*, 2012, **50**, 1583-1590.
2. A. V. Neimark, Y. Lin, P. I. Ravikovitch and M. Thommes, *Carbon*, 2009, **47**, 1617-1628.
3. X. Wu, W. Xing, J. Florek, J. Zhou, G. Wang, S. Zhuo, Q. Xue, Z. Yan and F. Kleitz, *Journal of Materials Chemistry A*, 2014, **2**, 18998-19004.
4. M. Dubinin, *Carbon*, 1989, **27**, 457-467.
5. A. Wahby, J. M. Ramos-Fernandez, M. Martinez-Escandell, A. Sepulveda-Escribano, J. Silvestre-Albero and F. Rodriguez-Reinoso, *ChemSusChem*, 2010, **3**, 974-981.
6. F. Stoeckli and L. Ballerini, *Fuel*, 1991, **70**, 557-559.
7. Z. Zhang, M. Xu, H. Wang and Z. Li, *Chemical Engineering Journal*, 2010, **160**, 571-577.
8. G. P. Hao, W. C. Li, D. Qian, G. H. Wang, W. P. Zhang, T. Zhang, A. Q. Wang, F. Schuth, H. J. Bongard and A. H. Lu, *Journal of the American Chemical Society*, 2011, **133**, 11378-11388.
9. G.-P. Hao, Z.-Y. Jin, Q. Sun, X.-Q. Zhang, J.-T. Zhang and A.-H. Lu, *Energy & Environmental Science*, 2013, **6**, 3740-3747.
10. N. P. Wickramaratne and M. Jaroniec, *Journal of Materials Chemistry A*, 2013, **1**, 112-126.
11. N. P. Wickramaratne, J. Xu, M. Wang, L. Zhu, L. Dai and M. Jaroniec, *Chemistry of Materials*, 2014, **26**, 2820-2828.
12. Y. Xia, R. Mokaya, G. S. Walker and Y. Zhu, *Advanced Energy Materials*, 2011, **1**, 678-683.
13. Y. Zhang, B. Li, K. Williams, W. Y. Gao and S. Ma, *Chemical communications*, 2013, **49**, 10269-10271.
14. S. Y. Lee and S. J. Park, *Journal of colloid and interface science*, 2013, **389**, 230-235.
15. N. P. Wickramaratne and M. Jaroniec, *ACS applied materials & interfaces*, 2013, **5**, 1849-1855.
16. M. Sevilla and A. B. Fuertes, *Journal of Colloid Interface Science*, 2012, **366**, 147-154.
17. L. Y. Meng and S. J. Park, *Journal of Colloid Interface Science*, 2010, **352**, 498-503.
18. M. Sevilla, P. Valle-Vigón and A. B. Fuertes, *Advanced Functional Materials*, 2011, **21**, 2781-2787.

19. G. P. Hao, W. C. Li, D. Qian and A. H. Lu, *Advanced materials*, 2010, **22**, 853-857.

20. Q. Li, J. Yang, D. Feng, Z. Wu, Q. Wu, S. S. Park, C.-S. Ha and D. Zhao, *Nano Research*, 2010, **3**, 632-642.

21. Y. Zhao, L. Zhao, K. X. Yao, Y. Yang, Q. Zhang and Y. Han, *Journal of Materials Chemistry*, 2012, **22**, 19726-19731.

22. J. Wang, A. Heerwig, M. R. Lohe, M. Oschatz, L. Borchardt and S. Kaskel, *Journal of Materials Chemistry*, 2012, **22**, 13911-13913.

23. C. Pevida, T. C. Drage and C. E. Snape, *Carbon*, 2008, **46**, 1464-1474.

24. M. Sevilla and A. B. Fuertes, *Energy & Environmental Science*, 2011, **4**, 1765-1771.

25. R. Banerjee, H. Furukawa, D. Britt, C. Knobler, M. O'Keeffe and O. M. Yaghi, *Journal of the American Chemical Society*, 2009, **131**, 3875-3877.

26. B. Wang, A. P. Cote, H. Furukawa, M. O'Keeffe and O. M. Yaghi, *Nature*, 2008, **453**, 207-211.

27. Q. Lin, T. Wu, S. T. Zheng, X. Bu and P. Feng, *Journal of the American Chemical Society*, 2012, **134**, 784-787.

28. J. An, S. J. Geib and N. L. Rosi, *Journal of the American Chemical Society*, 2009, **132**, 38-39.

29. W. Xing, C. Liu, Z. Zhou, L. Zhang, J. Zhou, S. Zhuo, Z. Yan, H. Gao, G. Wang and S. Z. Qiao, *Energy & Environmental Science*, 2012, **5**, 7323-7327.

30. Z. Zhang, J. Zhou, W. Xing, Q. Xue, Z. Yan, S. Zhuo and S. Z. Qiao, *Physical Chemistry Chemical Physics*, 2013, **15**, 2523-2529.